PCCP

PAPER

View Article Online
View Journal | View Issue

Cite this: *Phys. Chem. Chem. Phys.*, 2014, **16**, 26213

The effect of anatase crystal orientation on the photoelectrochemical performance of anodic TiO_2 nanotubes†

Próspero Acevedo-Peña,*[a] Federico González,[a] Gonzalo González[b] and Ignacio González[a]

Received 1st September 2014,
Accepted 10th October 2014

DOI: 10.1039/c4cp03930k

www.rsc.org/pccp

TiO_2 nanotube films were prepared by anodizing Ti plates in ethylene glycol based electrolytes containing variable concentrations of ammonium fluoride and water. The morphology, optical and semiconducting properties, as well as the composition of TiO_2 films were shown to be dependent on the anodizing bath composition. Among different film properties, only the preferential orientation of anatase crystals, quantified with the texture coefficient of the (004) plane, $TC_{(004)}$, showed the same dependence of photoelectrochemical performance on the electrolyte composition. The increased value of $TC_{(004)}$ was related to anatase crystals piling up in the [001] direction (normal to the plane of the Ti substrate), forming a fiber like texture structure along the tube that facilitates the transport of photogenerated electrons toward the conducting substrate.

Introduction

Since the work of Fujishima and Honda,[1] TiO_2 has been thoroughly studied for its application in photoelectrochemical cells due to its high stability and outstanding performance as an anode.[2–4] In order to improve the photoelectrochemical performance of TiO_2, different methodologies have been developed for its processing, having as a result films of different morphologies and properties that modulate the material's behavior.[5–9] In recent years, obtaining TiO_2 nanotubes by anodization in electrolytes containing fluoride ions has received huge attention due to the simplicity, reproducibility and high control of morphology.[10–12] It allows production of highly ordered structures that permit the directed electron transport towards the current collector and a high contact area with the electrolyte to carry out the oxidation reaction.

To design these structures and to provide more efficient anodes, it is necessary to understand different parameters that govern the photoelectrochemical performance of TiO_2 nanotube films. Their photoelectrochemical activity has been correlated with morphological parameters,[13] semiconducting properties,[14] and anatase crystallinity.[15] Recently, the possibility of controlling the orientation of anatase crystals in TiO_2 nanotubes in the [001] direction has been reported, as a function of H_2O concentration in ethylene glycol based electrolytes, which improves the film's photoelectrochemical performance.[16–19] This behavior has been correlated with a higher amount of anatase (001) facets exposed to the solution.[16–18] However, although the preferred orientation was corroborated by selected area diffraction patterns, the orientation degree of anatase crystals has been measured semi-quantitatively as a function of the ratio of anatase peaks corresponding to the (004) and (200) planes,[17] thereby being difficult for the detection of the real orientation degree of anatase crystals, and its relation to photoelectrochemical performance of the film. Also, even though other techniques can be used for determining crystallite orientation and distribution, such as transmission electron microscopy,[16–18] their main drawback is a relatively small area of analysis. On the other hand, the irradiation area on the sample surface in X-ray diffraction techniques goes from hundreds of square micrometers to hundreds of square millimeters. Furthermore, the penetration depth of conventional X-ray tubes in inorganic materials is tens of times higher than that of electrons possessing conventional energies in electronic microscopes. Thus, X-ray diffraction techniques allow the analysis of textural information of samples averaged over a large area and volume at the scale of some important devices using TiO_2.

There are different approaches to the film texture determination by XRD techniques. The most accessible is by performing a

[a] *Universidad Autónoma Metropolitana-Iztapalapa, Av. San Rafael Atlixco 186. Col. Vicentina, 09340, Ciudad de México, D.F., Mexico. E-mail: prosperoacevedopena@yahoo.com*

[b] *Instituto de Investigaciones en Materiales, Universidad Nacional Autónoma de México, Circuito Exterior S/N, A.P. 70-360, Ciudad de México, D.F., Mexico*

† Electronic supplementary information (ESI) available: Voltammetric characterization in the dark, XPS spectra, band-gap measurements from the Kubelka-Münk approach, semiconducting properties derived from Mott–Schottky plots, the Rietveld refinement of the XRD spectrum and estimation of the corrected $TC_{(004)}$ for nanotube shape. See DOI: 10.1039/c4cp03930k

conventional symmetrical reflection (CSR) measurement (as that obtained in the Bragg–Brentano geometry, in which diffraction comes only from lattice planes that are parallel to the sample surface), and then data analysis using the texture coefficient (TC). In this approach, texture characterization is achieved by comparing the observed relative peak intensity of representative Bragg reflections with those of a randomly-oriented powder standard of the same compound. However, for a strongly preferred-oriented thin film, especially that with a high morphological anisotropy, such as one having nanorods or nanotubes with a given crystallographic orientation along their longer axis, the CSR-TC approach may not be sufficient. In order to overcome this possible limitation, an alternative is to perform pole figure (PF) measurements. In this approach, the XRD is used, in particular, to determine crystallite orientation; so that, the film texture is directly obtained from the whole sample and not only from a small portion. Additionally, in films with a high morphological anisotropy, it is very useful to perform in-plane pole figure measurements. In such measurements, diffraction comes from lattice planes that are perpendicular or oblique to the sample surface, as is expected for the (101) anatase plane in a film with its crystallographic *c*-axis preferentially-oriented perpendicular to the substrate. Here, we have synthesized TiO_2 films by anodization in ethylene glycol based electrolytes with different concentrations of NH_4F, keeping a fixed concentration of H_2O, and with different concentrations of H_2O, keeping a fixed concentration of NH_4F, using the experimental strategy previously reported by the authors.[14,19,20] The morphology, optical and semiconducting properties, and surface composition of the films were characterized to correlate them with their photoelectrochemical water oxidation performance. Additionally, in order to determine the texture of the TiO_2 films, we have performed measurements by two different X-ray diffraction techniques. The orientation degree of anatase crystals was quantified by the texture coefficient for the (004) plane, $TC_{(004)}$, taking 10 characteristic peaks of anatase present in CSR XRD in the Bragg–Brentano geometry. Alternatively, in-plane XRD figure poles for (101) and (004) planes were measured to gain direct insight into preferential orientation.

1. Experimental

The TiO_2 nanotube films were obtained by potentiostatic anodization in a two electrode cell at 30 V for 2 h in ethylene glycol based electrolytes either with different NH_4F concentrations (0.05 M, 0.10 M and 0.20 M) keeping the water content constant at 1%, or with different percentages of water (1%, 5%, 10%, 25% and 50%) keeping the NH_4F concentration constant at 0.02 M. Pt (99.99%, Alfa Aesar) was employed as a counter electrode placed at 2 cm from the Ti foil (99.95%, Alfa Aesar). The electrolyte was stirred with a magnetic bar during anodization. Finally, the films were thoroughly cleaned with ethanol and Millipore water (18.2 MΩ cm), left to air dry, and heat treated in ambient air at 450 °C (10 °C min^{-1}) for 30 min to obtain anatase polymorph.[14]

SEM images were acquired using a JSM 7600F high field emission microscope, with an accelerating voltage of 10.0 kV. Morphological characteristics of the formed films were estimated using the iTEM software from Olympus soft imaging solutions. The UV-Vis diffuse reflectance spectra were measured using a Varian Cary 100 spectrometer equipped with an integrating sphere. XPS analyses were performed using a Thermo Scientific K-Alpha X-ray photoelectron spectrometer with a monochromatized Al Kα X-ray source (1487 eV). Since oxygen is the predominant element in these types of materials, the position of the O_{1s} peak at 531.0 eV was monitored on each sample to ensure that no binding energy shift due to charging had occurred. Narrow scans were collected at 60 eV analyzer pass energy and a 400 μm spot size. Additionally, the values obtained using the O_{1s} peak for charge compensation are closer to the TiO_2 reported values, 458.0 ± 0.4 eV,[21–26] than those obtained when the C_{1s} peak is used for charge compensation.

The X-ray diffractograms of the films were measured in air at room temperature using a Bruker D8 Advance diffractometer with the Bragg–Brentano θ–θ geometry, Cu-K_α radiation, a Ni 0.5% Cu-K_β filter in the secondary beam, and a one dimensional position sensitive silicon strip detector (Bruker, Lynxeye).[27,28] The diffraction intensity as a function of 2θ angle was measured between 20° and 70°, with a 2θ step of 0.020371°, for 38 s per point. Crystalline structures were refined by the Rietveld method using a fundamental parameters approach,[29] as implemented in the TOPAS code, version 4.2.27. The Cu-Kα X-ray emission profile was modeled with the one reported by G. Hölzer *et al.*[30] The parameters used during refinements included: polynomial terms for modeling background, lattice parameters and preferred orientation; and the width of a Lorentzian profile for modeling the average crystallite size. Last two features were modeled in reciprocal space with a symmetrized harmonics expansion.[31] The images of the shape of the average crystallite were generated using Medit software, release 2.3b,[32] following the methodology reported by Bokhimi *et al.*[33] The texture analysis was measured using a Rigaku Ultima IV X-ray diffractometer with a Cu-K_α radiation operating at 40 KV and 40 mA. The device has a CBO system (Cross Beam Optics) that determines a divergence angle of the output beam approximately at 0.03° and 0.05°. In-plane pole figures were recorded for poles (101) and (004) for three samples; the main advantage of such a method in comparison with the conventional Schultz reflection method is the possibility of recording practically the whole pole figure (*i.e.* from $\alpha = 0°$ to $\beta = 90°$). For α and β scans, sampling steps of 0.4° and 1.5° were adopted, with a speed of 90° min^{-1}.

The (photo)electrochemical tests were carried out in a conventional three electrode cell equipped with a quartz window allowing the UV light illumination of the entire portion (1.23 cm^2) of the TiO_2 nanotube film exposed to the electrolyte. An Ag/AgCl (3.0 M KCl) electrode was employed as a reference electrode and a graphite bar (99.999%, Alfa Aesar) as a counter electrode. The 0.1 M $HClO_4$ aqueous electrolyte used for film characterization was prepared by employing Millipore water (18.2 MΩ cm) and $HClO_4$ (JT Baker, 69%). Before each test, the electrolyte was bubbled with N_2 gas for 30 min and a N_2

atmosphere was preserved during the experiments. The illumination was made using a Newport Q Housing (Model 60025) equipped with a 100 W Hg arc lamp.[14]

The semiconducting properties of the films were estimated from Mott–Schottky plots. The space charge capacitance of the film was extracted from the high frequency time constant of the potentiostatic EIS spectra obtained at 50 mV intervals between 0.75 V *vs.* Ag/AgCl and 0.0 V *vs.* Ag/AgCl.[14] Prior to each measurement, the measuring potential was imposed for 10 minutes in order to stabilize the interfaces, then the EIS spectra were collected in a frequency interval between 10 kHz and 10 mHz with AC perturbation of ±10 mV (peak to peak). Finally, the experimental EIS spectra were fitted to an equivalent circuit, $R(Q(R(QR)))$, using Boukamp software.

The (photo)electrochemical characterization was carried out using a BAS Epsilon potentiostat and EIS measurements were performed in an EG&G PAR model 283 potentiostat/galvanostat, coupled to a SI model 1260 Solartron frequency response analyzer.

2. Results and discussion

2.1 TiO_2 nanotube film characterization

The morphology of the film obtained after 2 h of anodization at 30 V, without heat treatment, was characterized by SEM images. Top and cross sectional views of the films formed in different electrolytes are shown in Fig. 1. Variation in morphology of the films is in agreement with the variation in electrolyte aggressiveness, as has been reported in previous research studies.[20,34,35] The ordered TiO_2 nanotube films were obtained in all cases except for the electrolyte containing 0.20 M NH_4F and 50% H_2O (Fig. 1g), which exhibited a sponge like morphology due to considerably increased chemical attack suffered by nanotubes during anodization.

Table 1 Morphological parameters of the formed films estimated from SEM images. Internal diameter, d_i; tube length, l; wall thickness, w; tube to tube distance, d_t; porosity, P; roughness factor, R

$[NH_4F]$ (M)	$\%H_2O$	d_i[a] (nm)	l[a] (nm)	w[a] (nm)	d_t (nm)	P	R
0.05	1	58 ± 6	4878 ± 18	10.3 ± 2.1	71 ± 7	0.72	391.9
0.10	1	59 ± 9	4853 ± 47	10.4 ± 1.3	85 ± 11	0.71	383.4
0.20	1	58 ± 10	4536 ± 50	12.0 ± 1.8	84 ± 9	0.70	343.6
0.20	5	64 ± 7	2473 ± 49	11.5 ± 2.2	92 ± 12	0.71	180.6
0.20	10	77 ± 9	2343 ± 52	9.4 ± 1.2	100 ± 11	0.75	161.2
0.20	25	94 ± 11	2443 ± 56	9.6 ± 1.9	128 ± 16	0.77	144.1
0.20	50	—	1563 ± 34	—	—	—	—

[a] The values reported in the table are an average of 500 measurements for d_i and w and 100 measurements for l.

From SEM images similar to those shown in Fig. 1, different morphological parameters of TiO_2 films were estimated (Table 1): internal tube diameter (d_i), tube length (l), wall thickness (w), tube to tube distance (d_t), film porosity, P, estimated from eqn (1),[36] and the roughness factor, R, estimated from eqn (2).[37]

$$P = 1 - \frac{2\pi w(w + d_i)}{\sqrt{3}(d_i + 2w)^2} \quad (1)$$

$$R = 1 + \frac{4\pi l(w + d_i)}{\sqrt{3}(d_i + 2w)^2} \quad (2)$$

The increase in NH_4F concentration did not cause considerable variations in d_i and l, and had a slight influence on film porosity (Table 1). In contrast, the increase in H_2O content in the electrolyte provoked a considerable increase in d_i and a

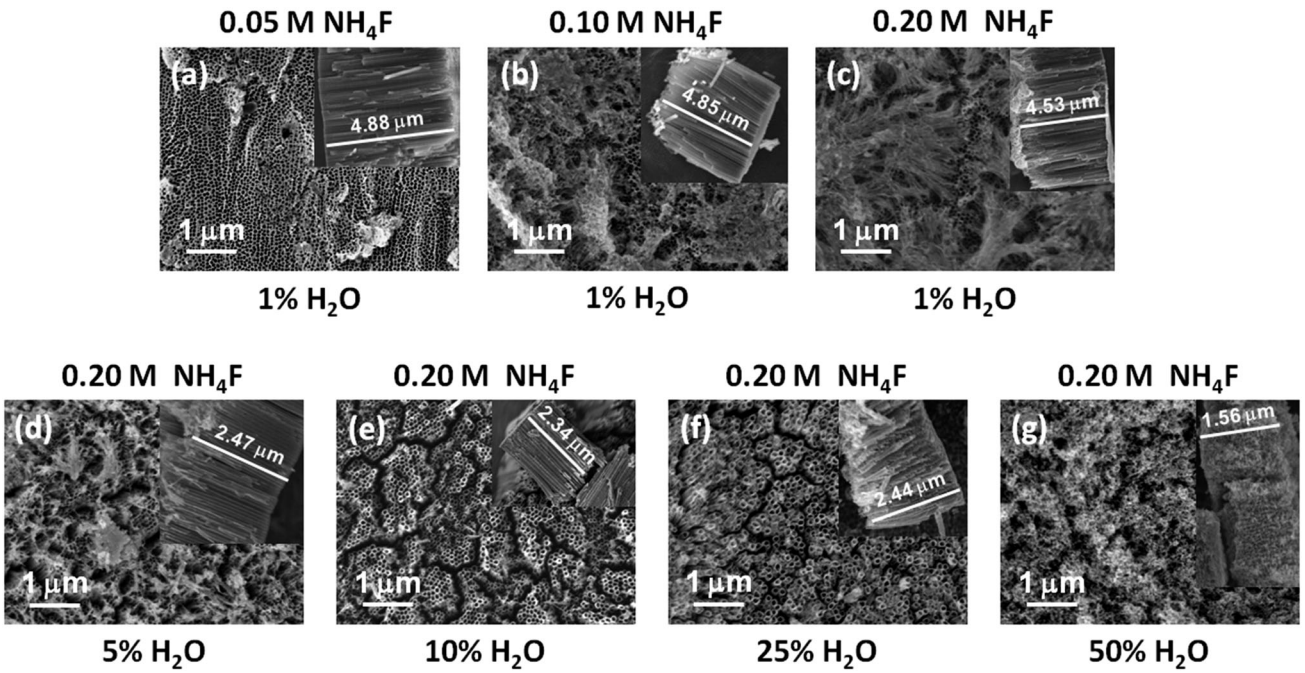

Fig. 1 Effects of NH_4F concentration and H_2O percentage (indicated in figure) on the morphology of the TiO_2 film obtained by anodization at 30 V for 2 h, without heat treatment.

decrease in both l and w, due to a higher chemical attack of the formed oxide resulting in the greater porosity of the formed film. The value of d_t increased with NH_4F concentration and H_2O content due to the dissolution of titanium oxifluoride film formed on the tube walls during its growth.[10–12,20] R, which represents the physical surface area of the film per unit of projected area, decreased as NH_4F concentration and H_2O content in the electrolyte increased. Voltammetric characterization (ESI,† Fig. S1) of the films heat treated at 450 °C for 30 min in the dark (10 °C min^{-1}) confirms an increase in the roughness factor of the films with the H_2O amount present in the anodizing bath, as well as in anodic currents measured during the reverse scan.[38] However, the variation in NH_4F concentration did not show considerable variations in the recorded currents, which is in agreement with the variation in R observed in Table 1. The correlation between R and voltammetric behavior of the film obtained in the dark indicates a variation in the electroactive area of the electrodes, particularly associated with the H_2O content in the anodizing bath during film synthesis.

The films obtained and heat treated at 450 °C for 30 min (10 °C min^{-1}) were characterized by XPS (ESI,† Fig. S2). The spectra show no variations in Ti (Ti_{2p}) and O (O_{1s}) species, but do show them in the presence of N and F species in porous TiO_2 films, particularly those obtained at higher NH_4F concentration and lower H_2O content. The presence of these species, mainly N,[39] modified the optical properties of the obtained films causing a variation in the band gap (E_g) measured from the reflectance spectra using the Kubelka–Münk approximation for the indirectly allowed transitions (ESI,† Fig. S3). On the other hand, semiconducting properties of the films estimated by Mott–Schottky curves also showed to be dependent on the anodizing bath composition (ESI,† Fig. S4). While a higher NH_4F concentration in the anodizing bath increases the number of N_d carriers in the film and considerably displaces E_{fb} towards less positive values, a higher H_2O content in the anodizing bath decreases N_d of the film maintaining its E_{fb} constant until a slight increase at 25% water content, a behavior similar to that previously reported by other researchers.[15]

Fig. 2 shows XRD patterns for all the prepared films after being heat treated at 450 °C for 30 min (10 °C min^{-1}). The only crystalline phase present in the films is anatase, but because of the thickness of these films, the X-ray beam penetrates until the substrate and titanium maximums also appear in diffractograms. Normally, the most intense peak for anatase is the one corresponding to the (101) plane, present at ~25.3°. However, at low NH_4F concentrations (Fig. 2i and ii), the peak corresponding to the (004) plane, present at ~38°, is much more intense than that of the (101) plane, which indicates that depending on the conditions for the growth of TiO_2 nanotubes, they may be preferentially oriented along certain crystallographic orientation, *i.e.*, they may exhibit a texture. Although this behavior has been already reported in previous works,[16–19] there is little knowledge of its origin and its impact on the performance and properties of the film.

In order to establish the effect of film growth conditions on the crystalline properties of nanotubes, our first approximation

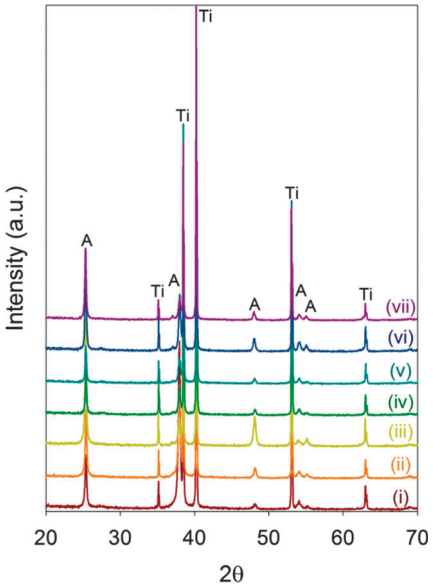

Fig. 2 XRD patterns of TiO_2 films (heat treated at 450 °C for 30 min) previously formed by potentiostatic anodization at 30 V for 2 h, in different electrolytes: (i) 0.05 M NH_4F, (ii) 0.10 M NH_4F, (iii) 0.20 M NH_4F in ethylene glycol with 1% H_2O, and 0.20 M NH_4F in ethylene glycol with (iv) 5% H_2O, (v) 10% H_2O, (vi) 25% H_2O and (vii) 50% H_2O.

was to extract intensities of 10 Bragg reflections appearing in the interval of 20° to 70° at 2θ, corresponding to anatase (Fig. 2).

These data were obtained from the Rietveld refinement of diffractograms, including the peaks attributed to Ti. The unit cell of anatase was modelled with tetragonal symmetry described by the space group I_{41}/amd, and a basis containing one Ti^{4+} at the relative coordinates (0, 0, 0) and one O^{2-} at the relative coordinates (0, 0, z) with an initial z value of 0.2. The hexagonal unit cell of metallic titanium (phase α) was modelled with the symmetry described by the space group P_{63}/mmc and a basis containing only one Ti atom at the relative coordinates (1/3, 2/3, 1/4). To show the good fit between the experimental and calculated X-ray diffractograms, a typical Rietveld refinement plot is depicted in Fig. S5 (ESI†) obtained for the film grown at 30 V for 2 h in an electrolyte containing 0.05 M NH_4F in ethylene glycol with 1% H_2O and heat treated.

An intensity ratio (I_{004}/I_{101}) of about 0.20 was determined from XRD measurements of a randomly oriented and isotropic

Table 2 Texture coefficient values of the (004) plane, $TC_{(004)}$, and I_{004}/I_{101} ratios of TiO_2 porous films grown in different anodizing baths

[NH_4F] (M)	%H_2O	$TC_{(004)}$[a]	I_{004}/I_{101}
0.05	1	6.94	3.79
0.10	1	5.57	1.69
0.20	1	2.19	0.32
0.20	5	3.81	0.84
0.20	10	4.17	1.00
0.20	25	4.03	0.80
0.20	50	2.66	0.50

[a] $TC_{(004)}$ estimated for anatase crystals randomly c-oriented in TiO_2 nanotubes is 2.41.

in shape commercial TiO_2 powder sample (Degussa P25), whereas the same ratio calculated from the intensities extracted from Rietveld refinements of XRD spectra of different TiO_2 films showed values ranging from 3.79 to 0.32 (see Table 2). As the I_{004}/I_{101} ratio in the TiO_2 porous films is 1.5 to 19 times bigger than for isotropic and randomly oriented powder, it is reasonable to assume that anatase crystals are preferentially oriented with their (001) planes parallel to the Ti-substrates as a function of the anodizing bath composition. Following the approach reported by Ariosa *et al.*,[40] a semi quantitative estimation of the texture can be calculated using the extracted intensities from the texture coefficient (TC), defined by eqn (3).[41]

$$\mathrm{TC}_{(xyz)} = \frac{I_{xyz}/I^0_{xyz}}{\frac{1}{N}\sum I_{hkl}/I^0_{hkl}} \quad (3)$$

where I_{hkl} represents the relative intensity for the (hkl) reflection, I^0_{hkl} is the relative intensity for the (hkl) reflection for isotropic randomly oriented powder and N is the number of Bragg reflections considered (10 in our case). By definition, TC ranges from 1 (no texture) to N (single oriented crystals).[40]

The texture coefficient for the (004) plane, $TC_{(004)}$, and the ratio I_{004}/I_{101} for films grown under different conditions are shown in Table 2. From data in Table 2 two facts are noteworthy: (1) $TC_{(004)}$ as well as the I_{004}/I_{101} ratio decrease as NH_4F concentration increases in the anodizing bath containing 1% H_2O and (2) films grown at 0.20 M NH_4F with the intermediate 10% H_2O value reach a maximum $TC_{(004)}$ (Table 2).

Further analysis (see ESI† for details) of the XRD data can be achieved by assuming that anatase crystals in TiO_2 nanotubes are preferentially assembled along the [001] direction of the tetragonal cell, *i.e.* they are *c*-axis oriented like nanotubes, though not fully oriented perpendicular to the substrate. According to eqn (S1) (ESI†), the intensity correction factor for the (004) peak is 1, while for the intensity of the (101) peak, which appears when the *c*-axis oriented nanotubes are tilted by $\psi_{101} = 68.3^\circ$, the intensity correction factor is 0.137. From ten calculated shape correction factors (one for each reflection) shown in Table S1 (ESI†), it is possible to calculate a corresponding $TC_{(004)}$ for anatase crystals randomly c-oriented in TiO_2 nanotubes at around 2.41.

For the sample grown with 0.2 M NH_4F/1% H_2O and 0.2 M NH_4F/50% H_2O and considering the presence of nanotubes, it can be stated that anatase crystals are randomly oriented, since the $TC_{(004)}$ values of 2.19 and 2.66, respectively (see Table 2), are very close to the value of $TC_{(004)}$ estimated for anatase crystals randomly c-oriented in TiO_2 nanotubes. In the other films, there is an additional contribution besides purely attributable to the anisotropy (nanotube morphology) of the films. This texture is due to the *c*-axis oriented piling of the anatase crystals in the nanotubes and to the preferential orientation of these along the perpendicular direction of the Ti substrate.

Generally speaking, pole figure measurement is an XRD technique where the diffraction angle (2θ) is fixed and the diffracted intensity is collected by varying two geometrical parameters: the α angle (the tilt angle from the sample surface normal direction) and the β angle (the φ rotation angle around the sample surface normal direction). The obtained diffracted intensity data are plotted as a function of α and β. Further experimental evidence of the *c*-axis oriented piling is provided in Fig. 3 through pole diagrams obtained for three different films: (a) 0.05 M NH_4F/1% H_2O, (b) 0.2 M NH_4F/1% H_2O, and (c) 0.2 M NH_4F/50% H_2O. Fig. 3 shows equal area projection plots of anatase for (101) and (004) poles. A fiber like texture along [001] is observed for all the films, associated with the nanotube morphology of the films. That means circular symmetry around some sample axis (Fig. 3), evidenced by a characteristic ring at $\alpha = 68.3^\circ$ (the angle between (101) and (004) planes). However, it is worth mentioning that for the sample grown in 0.05 M NH_4F/1% H_2O, the formation of just one ring was detected (Fig. 3a), unlike the other two films (Fig. 3b and c), where diffraction intensities are distributed around the ring, as shown by the changes in intensity. Consistently with the above, for (004) pole projections (Fig. 3d–f), only the central spot should appear, as it is the case; however, also the reflection from (002) of the Ti substrate overlaps and is strongly present with two spots, compatible with a $\{012\}\ \langle 12{-}1\rangle$ preferred orientation ($\alpha = 42.5^\circ$) of α Ti.

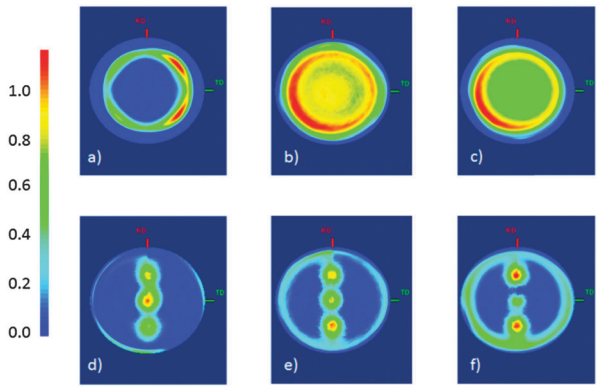

Fig. 3 Plots of equal area projections of anatase, (101) and (004) poles, characterized by a ring at $\alpha = 68.3^\circ$ and a central spot, respectively. These projections are compatible with a fiber texture along [001]. TiO_2 films (heat treated at 450 °C for 30 min) previously formed by potentiostatic anodization at 30 V for 2 h, in different electrolytes: 0.05 M NH_4F (1% H_2O) (plots (a) and (d)), 0.2 M NH_4F (1% H_2O) (plots (b) and (e)), and 0.2 M NH_4F (50% H_2O) (plots (c) and (f)).

Additionally to the previous texture analysis, and because of the size broadening effect on the XRD peaks was treated by spherical harmonic functions, it is possible to model the shape of the crystallites. The explicit formula for the spherical harmonics treatment of size broadening is expressed by the following equation:

$$\beta_{hkl} = \frac{\lambda}{D_{hkl}\cos\theta} = \frac{\lambda}{\cos\theta} = \sum_{lmp} a_{lmp}\, Y_{lmp}(\Theta_{hkl}, \Phi_{hkl}) \quad (4)$$

where β_{hkl} is the size contribution to the integral breadth of reflection (hkl), $Y_{lmp}(\Theta_{hkl}, \Phi_{\mathrm{hkl}})$ are spherical harmonic functions, and D_{hkl} is the Lorentzian crystallite size perpendicular to planes with hkl indices. Spherical harmonics (SH) up to the sixth order were used. For the anatase space group (I_{41}/amd) the physical meaning SH are Y_{00}, Y_{20}, Y_{40}, Y_{44+}, Y_{60} and Y_{64+}.

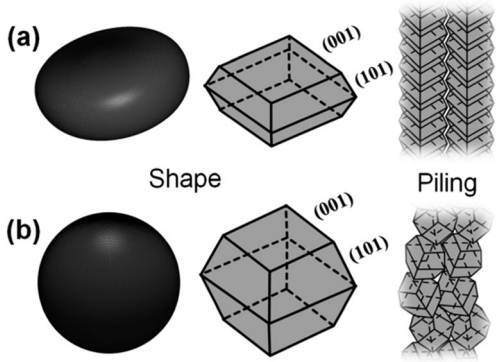

Fig. 4 Shape of the average anatase crystallite derived from the XRD line broadening treated by spherical harmonic functions for the TiO_2 films grown in: (a) 0.05 M and (b) 0.2 M NH_4F (1% H_2O). Also shown here are the schemes of the crystals and the piling based on the pole diagrams in Fig. 3.

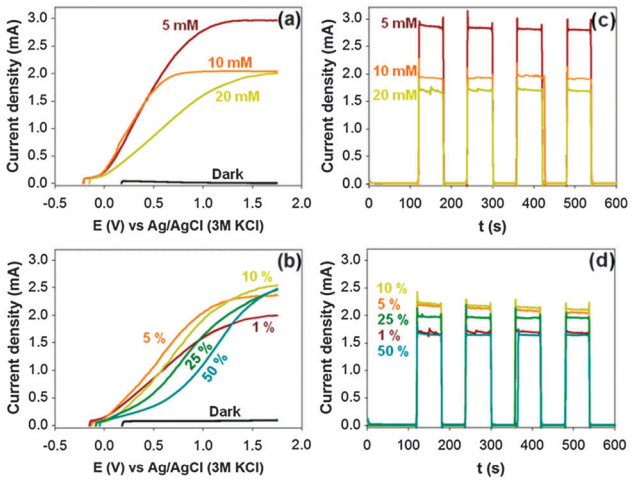

Fig. 5 Photoelectrochemical water oxidation performance (0.1 M $HClO_4$), measured by: (a and b) linear voltammetry (v = 20 mV s^{-1}) and (c and d) chronoamperometry (1.25 V *vs.* Ag/AgCl), for TiO_2 nanotube films previously grown at 30 V for 2 h in different electrolytes: (a) x mM NH_4F in ethylene glycol (1% H_2O) and (b) 0.20 M NH_4F in ethylene glycol (x% H_2O), and heat treated at 450 °C.

After refinements it is possible to estimate the apparent shape along each crystal direction. Fig. 4 shows the average shape of the crystallite derived from the XRD line broadening for the films grown in 0.05 M and 0.2 M NH_4F (1% H_2O). As can be seen, the disc shape of anatase crystallites in the film grown in 0.05 M NH_4F (Fig. 4a) that gives rise to a greater texture of the nanotubes allows the piling of many crystallites in the direction perpendicular to the Ti plate, as shown by the pole diagram in Fig. 3a. However, the shape of crystallites of the film grown in 0.2 M NH_4F (Fig. 4b), which exhibits less texture, is spherical. This is reasonable because although anatase crystals are piled up in the direction perpendicular to the Ti plate, no specific shape is necessary to allow the anisotropic piling. This proposal agrees with the findings reported by Lee *et al.*[17] using TEM characterization of TiO_2 nanotube films with oriented and randomly oriented anatase crystals. The selected area diffraction patterns of the nanotube cross section with oriented anatase crystals showed that the anatase crystals are piled up in the [001] direction, parallel to the *c*-axis of nanotubes.

2.2 Photoelectrochemical water oxidation performance

The effect of NH_4F concentration and H_2O content in the electrolyte used for the growth of TiO_2 films on their photoelectrochemical water oxidation performance was evaluated by measuring the photocurrent generated using linear voltammetry curves (Fig. 5a and b) and potentiostatic current transients (Fig. 5c and d).

The *I vs. E* curves obtained in a 0.1 M $HClO_4$ electrolyte in the absence (dark) and presence of illumination are shown in Fig. 5(a and b), for the films prepared in ethylene glycol based electrolytes with different NH_4F concentrations (Fig. 5(a)) and different H_2O contents (Fig. 5(b)). The currents measured in the dark are much lower than those measured in the presence of illumination, showing the considerable effect of illumination on the water oxidation process in TiO_2 porous films.

Additionally, potentiostatic current transients were measured by imposing an anodic potential of 1.25 V *vs.* Ag/AgCl, and intermittently illuminating the electrode. The measured *I vs. t* curves are shown in Fig. 5(c and d). After imposing the potential of 1.25 V *vs.* Ag/AgCl in the dark, a current rapidly decreasing over time was recorded. Upon illuminating the electrode, the current immediately increased and remained practically constant until the illumination was interrupted and got close to zero, as initially measured in the dark.

Although the disappearance of the nanograss and formation of well defined nanotubular structures (Fig. 1) were well correlated with the increase in photogenerated currents,[42] these only refer to outer changes in morphology of the films, leaving aside the inner changes suffered by the films during the processing. On the other hand, structural and compositional changes that influenced the observed response were also seen. For instance, the insertion of species from the electrolyte used for film anodization modified the optical and semiconducting properties of the films, particularly of that formed in the electrolyte containing 0.20 M NH_4F in ethylene glycol (1% H_2O). Previous studies have reported that N doping of TiO_2 leads to a decrease in E_g increasing its performance under visible light. However, this modification leads to a decreased performance of the material when it is illuminated with UV light, because oxygen vacancies created by N insertion in the material induce energy states below the conduction band, which modify the electron transport through the films.[39] Despite all this, none of these properties can be directly related to the variation in photoelectrochemical performance of TiO_2 films prepared in this study.

Different research studies have reported that the composition of the electrolyte employed for the growth of TiO_2 nanotubes seems to modify anatase crystallinity in nanotubes,[13] as well as its preferential orientation in the [001] direction,[16–19] having direct repercussions on its photoelectrochemical performance. Upon comparing the dependence between the measured photocurrent from chronoamperograms in Fig. 5 and $TC_{(004)}$ reported in Table 2, these two variables are seen to exhibit the same dependence on electrolyte composition, Fig. 6. It is worth mentioning that even when the data in Fig. 6

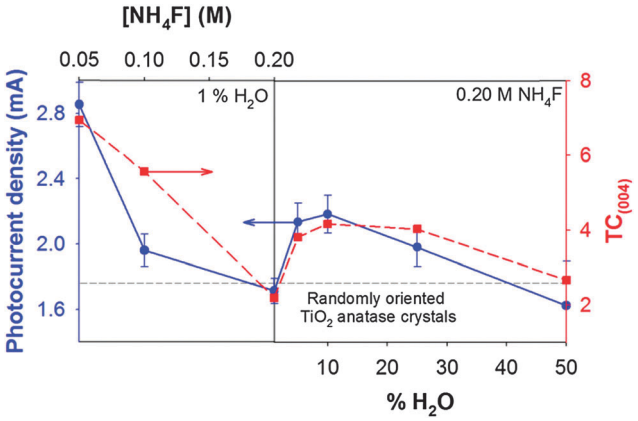

Fig. 6 Effects of anodizing bath composition on the measured photocurrent and texture coefficient $TC_{(004)}$ estimated from XRD in Fig. 4.

appear to follow only one tendency, these data comprise a wide change in the tube length and pore diameter, and a comparison must be done with restraint. For example, in the left part of Fig. 6 are plotted the data for films obtained in the anodic bath with lowest water content (1%) and different NH_4F concentrations. These films showed a similar length, porosity and roughness factor (see Table 1), but the preferential orientation of anatase crystals in the [001] direction seems to control the magnitude of the photocurrent measured and, furthermore, depolarize the water oxidation reaction, as observed in Fig. 5a, in which the photocurrent density rise at lower potentials for films with higher $TC_{(004)}$. On the other hand, the right part of Fig. 6 compares the photocurrent of films with different morphological properties, see Table 1, so the changes in the photocurrent cannot merely be assumed to alteration in $TC_{(004)}$, even when undoubtedly this factor contributes to the photoelectrochemical behaviour of the film.

It is worth mentioning that XRD is a bulk measurement and the whole sample is being evaluated compared with the SEM or TEM observation that only evaluates a small portion of the sample; in this way, the information obtained from the Rietveld refinement represents a trustable measurement of the orientation degree of anatase crystals.

The obtained results allow us to propose that preferential orientation of anatase crystals in *c*-axis, which gives rise to a fibrous like structure (Fig. 3), favors the transport of photogenerated electrons from the outer part of the tube towards the conducting substrate, thus being reflected in an increase in the recorded photocurrent. Therefore, the greatest performance shown by these highly ordered structures is not related to a greater exposure of anatase {001} facets[16–19] that favors the dissociative adsorption of H_2O,[43] but to the improved transport of photogenerated electrons. Further studies are necessary for more thorough understanding of the origin and consequences of preferential orientation of anatase crystals, in order to design more efficient TiO_2 photoanodes.

Conclusions

By varying NH_4F concentration and H_2O content in ethylene glycol based electrolytes, the morphology of the TiO_2 film obtained *via* anodization was considerably modified causing transition from a nanoporous structure to nanotubes with surface deposits, then to nanotubes and finally to a sponge like film. Furthermore, anatase crystals formed after heat treatment at 450 °C exhibited a preferential orientation along the (004) plane in the films formed in electrolytes containing low NH_4F concentrations (0.05 and 0.10 M), in spite of the possible orientation provided by the oxide film nanotubular structure for the growth of anatase crystals. On the other hand, film composition was also modified depending on the nature of the electrolyte used for its growth due to insertion of F and N from the electrolyte, which had repercussions on optical and semiconducting properties of TiO_2 films.

The photoelectrochemical water oxidation performance of TiO_2 films showed to be dependent on the composition of the electrolyte used to form the porous TiO_2 structure, which may be related to morphological and composition changes. However, the preferential orientation of anatase crystals, quantified by texture coefficient $TC_{(004)}$, was the only variable that showed the same dependence on photoelectrochemical performance as the electrolyte composition. This behavior is associated with anatase crystals piling as fibers along the tube in the [001] direction, normal to the plane of the Ti substrate that seems to facilitate the transport of photogenerated electrons towards the conducting substrate.

Acknowledgements

The authors are indebted to the CONACyT for their financial support to carry out this work (Projects CB 2008/105655 and INFR 2011 1 163250). The authors thank Patricia Castillo from Laboratorio Central de Microscopía Electrónica (UAM-I) for her assistance in SEM images, Luis Lartundo Rojas, PhD, from Centro de Nanociencias y Micro y Nanotecnologías (UPALM-IPN) for XPS measurements, and LDRX (T-128) UAM-I for XRD measurements.

Notes and references

1 A. Fujishima and K. Honda, *Nature*, 1972, **238**, 37–38.
2 A. L. Linsebigler, G. Lu and J. T. Yates, *Chem. Rev.*, 1995, **95**, 735–758.
3 J. T. Carneiro, A. R. Almeida, J. A. Moulijn and G. Mul, *Phys. Chem. Chem. Phys.*, 2010, **12**, 2744–2750.
4 M. A. Henderson, *Surf. Sci. Rep.*, 2011, **66**, 185–297.
5 G. Waldner and J. Krýsa, *Electrochim. Acta*, 2005, **50**, 4498–4504.
6 M. Radecka, A. Trenczek-Zajac, K. Zakrzewska and M. Rekas, *J. Power Sources*, 2007, **173**, 816–821.
7 P. Acevedo-Peña, G. Vázquez, D. Laverde, J. E. Pedraza-Rosas, J. Maríquez and I. González, *J. Electrochem. Soc.*, 2009, **156**, C377–C386.
8 F. Zhu, H. Dong, Y. Wang, D. Wu, J. Li, J. Pan, Q. Li, J. Zhang and D. Xu, *Phys. Chem. Chem. Phys.*, 2013, **15**, 17798–17803.
9 L. Cái, I. S. Cho, M. Logar, A. Mehta, J. He, C. H. Lee, P. M. Rao, Y. Feng, J. Wilcox, F. B. Prinz and X. Zheng, *Phys. Chem. Chem. Phys.*, 2014, **16**, 12299–12306.

10 P. Roy, S. Berger and P. Schmuki, *Angew. Chem., Int. Ed.*, 2011, **50**, 2904–2939.
11 I. Paramasivam, H. Jha, N. Liu and P. Schmuki, *Small*, 2012, **8**, 3073–3103.
12 B. Chen, J. Hou and K. Lu, *Langmuir*, 2013, **29**, 5911–5919.
13 S. Liang, J. He, Z. Sun, Q. Liu, Y. Jiang, H. Cheng, B. He, Z. Xie and S. Wei, *J. Phys. Chem. C*, 2012, **116**, 9049–9053.
14 P. Acevedo-Peña and I. González, *J. Electrochem. Soc.*, 2013, **160**, H452–H458.
15 L.-K. Tsui, T. Homma and G. Zangari, *J. Phys. Chem. C*, 2013, **117**, 6979–6989.
16 M.-H. Jung, M.-J. Chu and M. G. Kang, *Chem. Commun.*, 2012, **48**, 5016–5018.
17 S. Lee, I. J. Park, D. H. Kim, W. M. Seong, D. W. Kim, G. S. Han, J. Y. Kim, H. S. Jung and K. S. Hong, *Energy Environ. Sci.*, 2012, **5**, 7989–7995.
18 Z. Yang, Z. Ma, D. Pan, D. Chen, F. Xu and S. Chen, *Ceram. Int.*, 2014, **40**, 173–180.
19 P. Acevedo-Peña, J. E. Carrera-Crespo, F. González and I. González, *Electrochim. Acta*, 2014, **140**, 564–571.
20 P. Acevedo-Peña, L. Lartundo-Rojas and I. González, *J. Solid State Electrochem.*, 2013, **17**, 2939–2947.
21 A. F. Carley, P. R. Chalker, J. C. Riviere and M. W. Roberts, *J. Chem. Soc., Faraday Trans. 1*, 1987, **83**, 351–370.
22 B. Siemensmeyer and J. W. Schultze, *Surf. Interface Anal.*, 1990, **16**, 309–314.
23 R. L. Kurtz and V. E. Henrich, *Surf. Sci. Spectra*, 1998, **5**, 179–181.
24 Z. Xia, H. Nanjo, T. Aizawa, M. Kanakubo, M. Fujimura and J. Onagawa, *Surf. Sci.*, 2007, **601**, 5133–5141.
25 I. Milošev, T. Kosec and H.-H. Strehblow, *Electrochim. Acta*, 2008, **53**, 3547–3558.
26 P. Acevedo-Peña, J. Vázquez-Arenas, R. Cabrera-Sierra, L. Lartundo-Rojas and I. González, *J. Electrochem. Soc.*, 2013, **160**, C277–C284.
27 W. Dabrowski, P. Grybos, P. Hottowy, K. Swientek and P. Wiacek, *Nucl. Instrum. Methods Phys. Res., Sect. A*, 2003, **512**, 213–219.
28 R. W. Cheary and A. A. Coelho, *J. Appl. Crystallogr.*, 1992, **25**, 109–121.
29 *TOPAS V4.2: General profile and structure analysis software for powder diffraction data. User's manual*, Bruker AXS, Karlsruhe, Germany, 2009.
30 G. Hölzer, M. Fritsch, M. Deutsch, J. Härwig and E. Föster, *Phys. Rev. A: At., Mol., Opt. Phys.*, 1997, **56**, 4554–4568.
31 M. J. Järvinen, *J. Appl. Crystallogr.*, 1993, **26**, 525–531.
32 P. Frey, *MEDIT: an interactive mesh visualization software, Technical Report RT-0253*, Institut National de Recherche en Informatique et en Automatique, 2001.
33 X. Bokhimi and R. Zanella, *J. Phys. Chem. C*, 2008, **112**, 12463–12467.
34 S. Yoriya and C. A. Grimes, *J. Mater. Chem.*, 2011, **21**, 102–108.
35 S. Yoriya, N. Bao and C. A. Grimes, *J. Mater. Chem.*, 2011, **21**, 13909–13912.
36 A. G. Kontos, A. I. Kontos, D. S. Tsoukleris, V. Likodimos, J. Kunze, P. Schmuki and P. Falaras, *Nanotechnology*, 2009, **20**, 045603.
37 K. Shankar, J. I. Basham, N. K. Allam, O. K. Varghese, G. K. Mor, X. Feng, M. Paulose, J. A. Seabold, K.-S. Choi and C. A. Grimes, *J. Phys. Chem. C*, 2009, **113**, 6327–6359.
38 M. Jankulovska, I. Barceló, T. Lana-Villarreal and R. Gómez, *J. Phys. Chem. C*, 2013, **117**, 4024–4031.
39 M. V. Dozzi and E. Selli, *J. Photochem. Photobiol., C*, 2013, **14**, 13–28.
40 D. Ariosa, F. Elhordoy, E. A. Dalchiele, R. E. Marotti and C. Stari, *J. Appl. Phys.*, 2011, **110**, 124901.
41 C. Barret and T. B. Massalski, *Structure of Metals*, Pergamon, Oxford, 1980, pp. 1923–1924.
42 D. Kim, A. Ghicov and P. Schmuki, *Electrochem. Commun.*, 2008, **10**, 1835–1838.
43 M. Sumita, C. Hu and Y. Tateyama, *J. Phys. Chem. C*, 2010, **114**, 18529–18537.

